Microstructure Evolution in AISI 430 Ferritic Stainless Steel Welds Treated with Aluminum and Titanium Powder Mixture

M.O.H. Amuda[1*] F.T. Lawal[1] and S. Mridha[2]

[1]Materials Development and Processing Research Group, Department of Metallurgical and Materials Engineering, University of Lagos, Lagos, Nigeria 101017
[2]Department of Mechanical and Aerospace Engineering, University of Strathclyde, G11XJ, Glasgow UK
[*]Corresponding author email: mamuda@unilag.edu.ng

Abstract
Ferritic stainless steel particularly the AISI 430 standard grade is a candidate material for radiation shielding in nuclear reactors for power generation at competitive cost than the workhorse AIS1 316L austenitic grade. But its widespread application as the next generation energy material in nuclear reactor is limited by the loss in mechanical properties arising from grain coarsening and other phase transformations in the heat affected zone of the material post-fusion welding. Thus, in this work, attempt was made to resolve the challenge of grain coarsening in fusion welded AISI 430 ferritic stainless steel for improved mechanical properties. Specifically, the ductility and tensile strength of AISI 430 ferritic stainless steel welds treated with mixture of aluminum and titanium powder was investigated in relation to the microstructural evolution in the weld. The columnar structure in the as-welded condition transited to equiaxed grain with lower percentage of delta ferrite in the powder-mixture treated welds. In this condition, the ductility and the tensile strength of the treated weld marginally improved by 5 percent. The present work in relation to existing work in this space established that powder mixture of aluminum and titanium is capable of producing defect free structural welds in ferritic stainless steel though with marginal improvement in mechanical properties.

Keywords: Delta ferrite, ductility, ferritic stainless steel welds, grain refinement, microstructure evolution

1.0 INTRODUCTION

Stainless steels are broadly considered as excellent materials for several applications in power generation particularly for electricity generation from nuclear sources (Lo *et al*., 2009). Whilst the austenitic stainless steel grade has been the workhorse of the stainless steel family for power generation, it has been established that it is not suitable for nuclear power reactor systems. This is because the material exhibits poor radiation shielding characteristics resulting in severe radiation damage to the material during fusion neutron reactions (Büyükyıldız *et al*., 2017). However, ferritic stainless steel grade is credited with excellent radiation shielding characteristics which commends the material for application in nuclear reactor for power generation. In addition to this, the material equally exhibits better stress-corrosion cracking resistance than the austenitic variety particularly in caustic environment. (Amuda *et al*., 2017; Cortie and Du Toit, 2016). Further, the material is a better choice where nickel undergoes leaching such as thermal reactor and cookware (Baldev *et al*., 2013; Kamerud *et al*., 2013).

The chemistry of ferritic stainless steel is characterized by the absence of nickel, a very costly constituent in the austenitic grade (Amuda *et al*., 2016; Amuda, 2011). The absence of nickel in ferritic stainless steel makes the material a low-cost alternative to austenitic stainless steel. Thus, ferritic stainless steel finds applications in several areas hitherto exclusive to austenitic stainless steel more particularly in nuclear reactor for radiation shielding.

Though there is a growing interest in the deployment of ferritic stainless steel for structural application, but this is limited by the inability to produce defect free structural welds of the

material. Literature has established that the fusion welding of ferritic stainless steels particularly the first-generation medium chromium grade generates many undesirable phenomena in the material such as grain coarsening and precipitation of chromium carbide (Delgado *et al*., 2015; Klas, 2012; Anbazhagan and Nagalakshmi, 2002). These phenomena induce poor mechanical and corrosion properties in the resulting fusion welds.

It is thus envisaged that controlling the phenomena of grain coarsening and carbide precipitation may assist in improving the weldability of ferritic stainless steel. There are many techniques that have been reported in the literature for accomplishing improved weldability in the material. A detailed review of these techniques is documented in relevant literature (Amuda and Mridha, 2010). Among the several techniques described in the literature, grain refinement techniques have been identified for generating substantial equiaxed grains in ferritic stainless steel welds with improved mechanical properties. Such treatments have also been credited with better solidification cracking resistance.

Grain refinement accomplished by additions of elements with similar atomic size to iron such as Al, Cu and V have been reported (Cavazos, 2006). In some other works, titanium and aluminum have been used for grain refinement in ferritic stainless steel. In one of such works, Villafuerte *et al*. (1990) accomplished grain refinement in ferritic stainless steel welds treated with different amounts of aluminum and titanium. The work established that equiaxed grains in the welds are enhanced by increasing welding speeds as well as the amount of aluminum and titanium. This work though provided a conceptual framework for accomplishing grain refinement in ferritic stainless steel welds, it is limited in scope because the grain refinement was accomplished on experimental steel with constitutive presence of aluminum and titanium rather than elemental. The implication of this is that costly bulk alloying would be needed to produce the experimental constitutive ferritic stainless steel whereas the phenomenon of grain coarsening is limited to the weld region not the bulk of the material. Thus, a non-bulk approach for the introduction of alloying elements into the weld pool of base metal was developed by incorporating the elements in powder form in electrode flux coatings for welding process using consumable electrode. The incorporated metal powder in the electrode coatings not only control the energy input into the base metal during fusion melting, it equally serves as nucleation sites for the resolidification of the molten weld pool. This enables the formation of equiaxed grains post-resolidification of the weld pool.

Electrode flux coating for the incorporation of elemental powder for grain refinement is not appropriate for autogenous non-filler process like the GTA welding process. Amuda *et al.* (2018) and Amuda (2011) developed a simple yet innovative technique for the incorporation of metal powder into the weld pool of ferritic stainless steel to enhance grain refinement. In this technique, specific concentration of aluminum and titanium metal powder was individually preplaced onto the substrate of the material before welding for grain refinement. These works reported appreciable grain refinement in the resolidified weld of ferritic stainless steel but there were substantial cracks in welds treated with titanium powder whereas no such crack was observed in aluminum treated welds. Thus, additional simultaneous injection of aluminum during the incorporation of titanium in the weld pool of ferritic stainless steel may assist to enhance microstructural stability in the welds. Villafuerte *et al.* (1990) demonstrated this postulation using experimental ferritic stainless in which titanium and aluminum were introduced during bulk alloying but the process is expensive and cumbersome.

Therefore, it is considered that incorporating a mixture of aluminum and titanium powder in the weld pool of ferritic stainless steel via a simple yet innovative technique of powder preplacement may equally achieve crack free grain refinement in GTA-welded ferritic stainless steel as accomplished by Villafuerte *et al*. (1990). Thus, the thrust of the current work is to produce defect free grain refined equiaxed weld in medium chromium ferritic stainless steel treated with mixture of aluminum and titanium via elemental metal powder preplacement technique in autogenous GTA welding process.

2.0 MATERIALS AND METHOD

2.1 Materials Preparation

1.5 mm thick medium chromium ferritic stainless steel material procured as AISI 430 commercial grade was used for the study. The composition of the material as provided in the materials safety data sheet and complemented with energy dispersive X-ray fluorescence (EDXRF) is presented in Table 1. Ti and Al powders of 99.9% purity and particle sizes of 3 and 15 µm respectively were used as grain refining agents. The AISI 430 ferritic stainless steel material of 1000 mm x 1000 mm sheet size was sectioned into coupon of dimensions 150 mm x 90 mm. The coupons were subsequently pre-cleaned in a Branson 2500 ultrasonic cleaner for 5 minutes; after which, they were prepared for powder injection by roughening with 300 grit size silicon carbide paper. A paste containing different amounts of the metal powder was prepared in a solution of polyvinyl alcohol (PVA) organic binder in accordance to the protocol established by Amuda et al. (2011). A pre-mixed Al and Titanium powder in different amounts were preplaced on the coupons' substrates using preplacement technique (Amuda, 2011). The coupons treated with preplaced powder mix were then placed in an oven at 60^{o}C for 24 hours to drive off moisture from the coupons.

Table1: Chemical composition of AISI 430 ferritic stainless steel provided by the supplier and complemented with EDXRF spectroscopy

Material	Composition (wt %)									KFF	Cr_{eq} / Ni_{eq}
	C	Cr	Si	Mn	P	S	Ni	Ti	Fe		
AISI 430 FSS	0.12	6.19	0.75	-	0.04	0.30	-	-	Balance	14.7	3.85

2.2. Experimental Procedure

Miller-Telwin 165 direct current automatic GTA welding machine with programmable torch movement was used to deposit autogenous single pass full penetration bead-on-plate welds on the prepared coupons in argon gas shielded environment. Process parameter selection was based on a Box-Behnken experimental design in which arc current, arc transverse speed and amount of powder were the basic variables. The details of the experimental set-up and the generic melting conditions are presented in Figure 1 and Table 2, respectively. The specific process parameter combination is listed in Table 3. The coupons were prepared for post-weld microstructural examination by sectioning them in direction normal to the weld interface using electrical discharge machining (EDM).

Metallographic preparation was conducted using conventional technique provided in the literature. Detailed examinations of the microstructure were made using Nikon Epiphot 200 light optical microscope incorporated with IMT image analysis software. The image analysis software was used for estimating both the grain size and the volume fraction of the phases in

accordance to ASTM JEOL JSM 5600 scanning electron microscope was used for fractography examination. Shimadzu XRD 6000 diffractometer was used to identify the phases present in both the base metal and weld section.

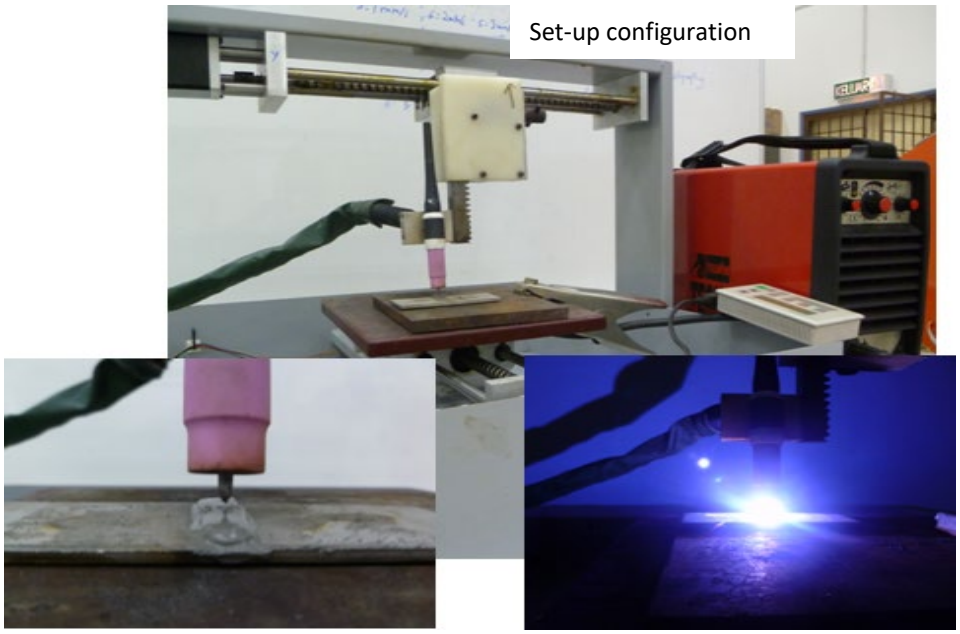

Figure 1. Experimental set-up of elemental powder addition via preplacement technique (Amuda *et al.*, 2018)

Microhardness was conducted on the coupons at a test load of 500g for a residence time of 10s with Mitutoyo MVK-H2 Vickers digital microhardness machine. The welded coupons were prepared for tensile testing using EDM wirecut. Transverse tensile test was conducted at room temperature on Shimadzu Trapezium AGX-250 electro-mechanically controlled universal testing machine at a cross head speed of 5mm/min.

Table 2: Melting Conditions (Amuda *et al.*, 2018)

Process	DCEN straight polarity full bead on plate penetration GTA weld
Position	Flat
Melting Conditions	
Current	70, 90, 110A
Voltage	30V
Speed	2.5-3.5 mm/s
Arc length	1.5mm
Elemental Powder	Al (0.08-0.16), Ti (0.18-0.39), Al+Ti (0.26-0.55) mg/mm2
Torch orientation	Vertical
Electrode configuration	2.44mm W-2 pct. Th., 600 cone included angle
Electrode stick-out	3mm
Shielding environment	99.9 pct. argon at a flow rate of 0.72L/min

Table 3: Process parameter combination for TIG torch melting of Al+Ti powder mix onto AISI 430 FSS welds

Weld run	I (A)	υ (mm/s)	V (V)	EI (J/mm)	Ar flow rate (L/min)	Type of powder	Powder content (mg/mm^2)
1	90	2.5	30	518	0.72	Al + Ti	0.13
2	70	3.0	30	336	0.72	Al + Ti	0.13
3	110	3.0	30	528	0.72	Al + Ti	0.13
4	90	3.5	30	370	0.72	Al + Ti	0.13
5	70	2.5	30	403	0.72	Al + Ti	0.20
6	110	2.5	30	634	0.72	Al + Ti	0.20
7	90	3.0	30	432	0.72	Al + Ti	0.20
8	70	3.5	30	288	0.72	Al + Ti	0.20
9	110	3.5	30	453	0.72	Al + Ti	0.20
10	90	2.5	30	518	0.72	Al + Ti	0.28
11	90	3.5	30	370	0.72	Al + Ti	0.28
12	110	3.0	30	528	0.72	Al + Ti	0.28
13	70	3.0	30	336	0.72	Al + Ti	0.28

3.0 RESULTS AND DISCUSSION

3.1 Macrostructural Features of the Welds

Figure 2 shows the track profiles in welds treated with mixture of aluminum and titanium powder in relation to the convention welds. The powder mixture treated welds demonstrate smooth narrow continuous track devoid of blisters unlike the broad and blister-like track in the conventional welds. This is in contrast to the discontinuous tracks and cracks previously obtained in titanium powder treated ferritic stainless steel welds (Amuda *et al.,* 2018).

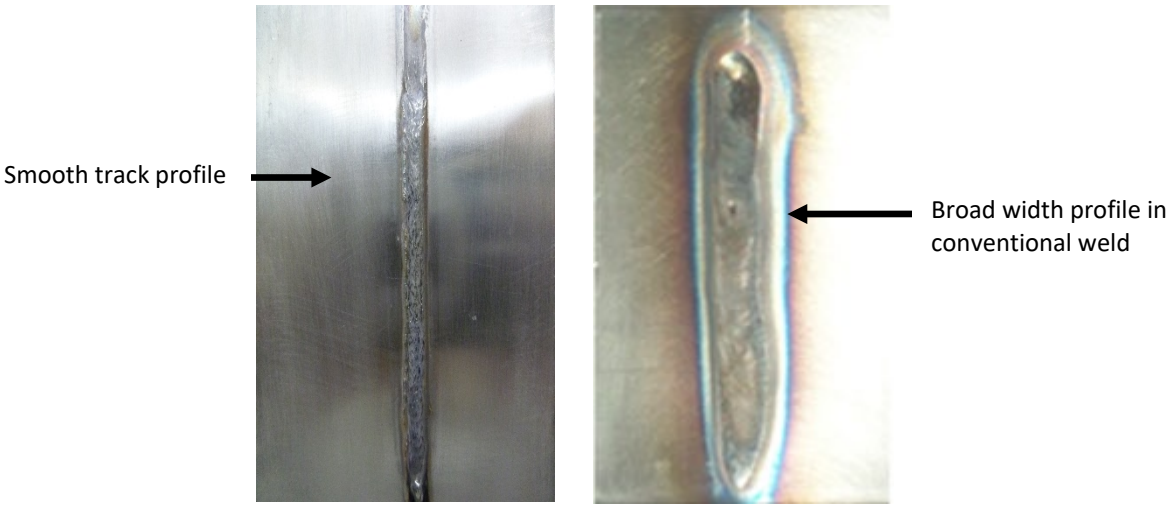

Figure 2. Track surface profiles in: (a) powder mixture treated ferritic stainless steel weld and (b) conventional weld (CW) at an energy input of 452 J/mm

The macrostructures of the powder mixture welds in relation to conventional weld are shown in Figure 3. The figure shows a narrower width and shallow depth in powder mixture treated welds in relation to the conventional welds. This is apparent absence of crack in the powder

mixture treated welds unlike what was obtained in a previous study on titanium powder treated ferritic stainless steel welds. There is no specific trend in terms of the concentration of powder on the shape of the weld. The macro-grains alignment in the conventional welds appears to project in the lateral direction suggesting the direction of heat dissipation in the welds. No such clear macro-grain alignment is visible in powder mixture treated welds.

The width-depth dimensions of the welds acquired using Nikon MM-400L trinocular head measuring microscope are shown in Table 4. The table showed that the size of the heat affected zone (HAZ) decreases with increase in the concentrations of powder mixture relative to the conventional weld. The average constriction in the HAZ geometry in this instance was about 43% whilst the fusion zone (FZ) had no specific relationship to the concentration of the powder introduced into the weld pool.

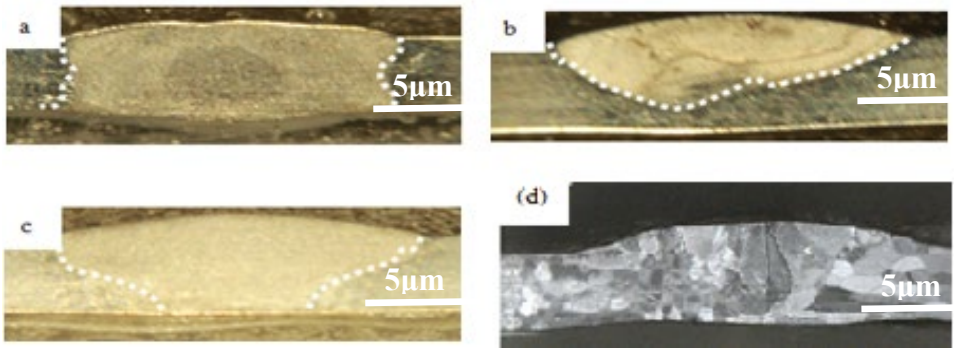

Figure 3. Macrostructure of welds treated with different concentrations of mixture of aluminum +titanium powders: (a) 0.26 mg/mm^2, (b) 0.2 mg/mm^2, (c) 0.39 mg/mm^2, (d) conventional weld (CW)

Table 4: Width-depth dimensions in welds at different concentrations of aluminum and titanium powder mixture

Weld No	I (A)	Speed (mm/s)	Voltage (V)	Heat Input (J/mm)	Normal Weld (mm)		Al +Ti Conc. (mg/mm^2)	Weld Geometry (mm)	
					FZ	HAZ		FZ	HAZ
AT1	70	3	30	336	3.41	1.72	0.26	4.24	0.90
AT2	90	2.5	30	518	5.9	2.07	0.26	4.81	1.15
AT3	90	3.5	30	370	3.76	1.58	0.26	3.90	1.10
AT4	110	3	30	528	7.34	2	0.26	4.99	1.23
AT5	70	2.5	30	403	3.78	1.83	0.40	3.77	0.71
AT6	70	3.5	30	288	3.05	1.52	0.40	2.81	0.75
AT7	90	3	30	432	5.42	1.84	0.40	4.56	1.16
AT8	110	2.5	30	634	7.89	2.4	0.40	6.17	1.23
AT9	110	3.5	30	453	5.88	1.61	0.40	5.62	0.75
AT10	70	3	30	336	3.41	1.72	0.55	3.19	1.00
AT11	90	2.5	30	518	5.9	2.07	0.55	4.64	1.17
AT12	90	3.5	30	370	3.76	1.58	0.55	3.96	1.02
AT13	110	3	30	528	7.34	2	0.55	6.55	1.41

3.2 Phase Identification in Powder Mixture Treated Welds

Phase characterisation in the resolidified melt pool conducted via XRD analysis is shown in Figure 4. The phases in the weld identified via powder diffraction file (PDF) searching and matching are indicated in the figure. The phases identified in the powder mixture treated welds are different from those in the conventional welds (martensite and chromium carbide precipitates). The spectra indicate that the phases present in the powder mixture treated welds are delta-ferrite, $AlTi_3C$, Al_3Ti and $AlTi_3$. The intermetallic phases in the welds are formed through in-situ reaction during melting (Sarker, 2010).

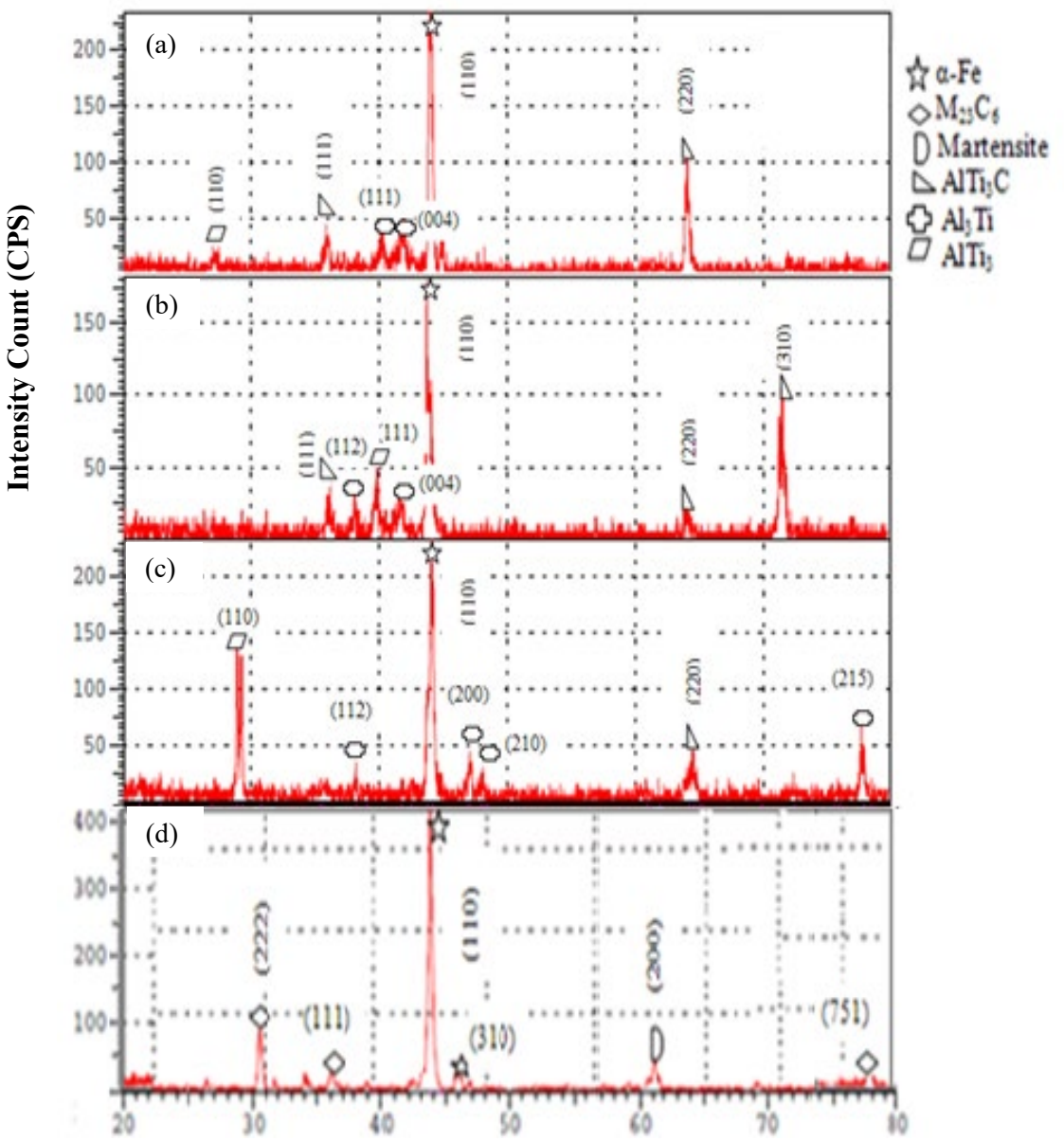

Figure 4. XRD spectra in Al + Ti powder mixture treated welds: (a) 0.13 mg/mm^2, (b) 0.20 mg/mm^2 and (c) 0.28 mg/mm^2 and (d) conventional weld

The figure equally shows the absence of diffraction peaks corresponding to martensite and $M_{23}C_6$-type carbide in the powder treated welds. This suggests that these powders may offer a strategy for avoiding the precipitation of $M_{23}C_6$-type carbide ($Cr_{23}C_6$). This stabilizes the chromium for sustained corrosion resistance.

3.3 Analysis of Microstructure of Powder Mixture Treated Welds

Figure 5 is the microstructure of the as-received base metal revealing equiaxed grains elongated in the rolling direction. The phases in the microstructure are considered comprise ferrite and networks of carbide at the grain boundary. Amuda et al. (2018) had reported in a recent work that the microstructures of the conventional welds comprise ferrite (α + δ), martensite (α') and chromium carbide ($Cr_{23}C_6$) precipitates. The grain structure in the conventional welds reveals columnar grains elongated in the direction of solidification.

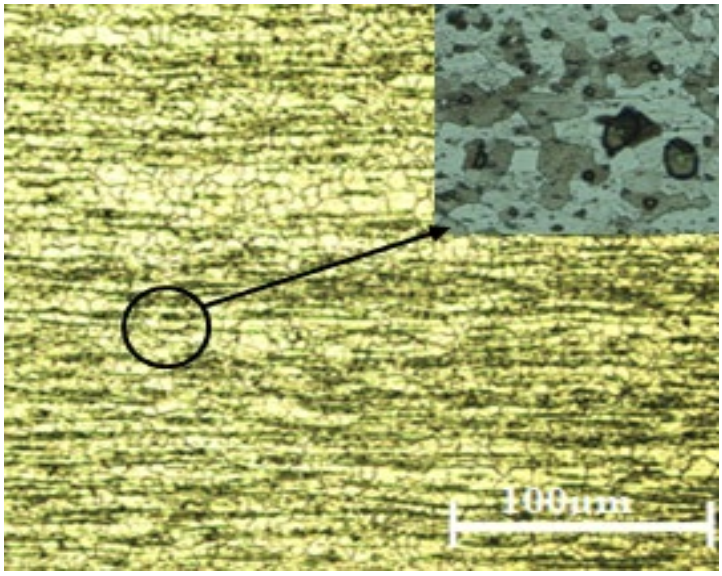

Figure 5. Optical micrograph of ferritic stainless steel base metal; insert shows ferrite and carbide phases (Amuda *et al*., 2018)

The microstructure of welds treated with different concentrations of the mixture of aluminum + titanium is presented in Figure 6 for comparison with the conventional weld. The microstructures in 0.26 and 0.40 mg/mm^2 powder mixture treated welds are free of defects however there are cracks in that of 0.55 mg/mm^2 of powder mixture. However, the grain structure in the microstructures is equiaxed and refined relative to the conventional welds. The microstructures show inhomogeneous distribution of dendrite at powder concentration of 0.26 and 0.55mg/mm2. The inhomogeneous distribution observed in the microstructures is believed to be due to the formation of flow loop in the melt (shown in Figure 7) which carries the preplaced powder into the melt pool. This flow pattern has been similarly reported in titanium-aluminide coating produced on titanium substrate (Mridha *et al*., 2001) and laser nitriding of commercial titanium (Mridha and Baker, 1994).

Published works attributes the formation of such flow pattern in the melt pool to marangoni convectional fluid flow (Kou, 2003; Lancaster, 1993). Additionally, weld treated with powder mixture exhibits about 20 percent increase in delta ferrite (Figure 8). Such increase in delta ferrite distribution in welds has been attributed to reduction in mechanical properties (Lippold and Kotecki, 2005). Thus, in the present work, it is postulated the increase in delta ferrite distribution may impair the mechanical properties of the weld.

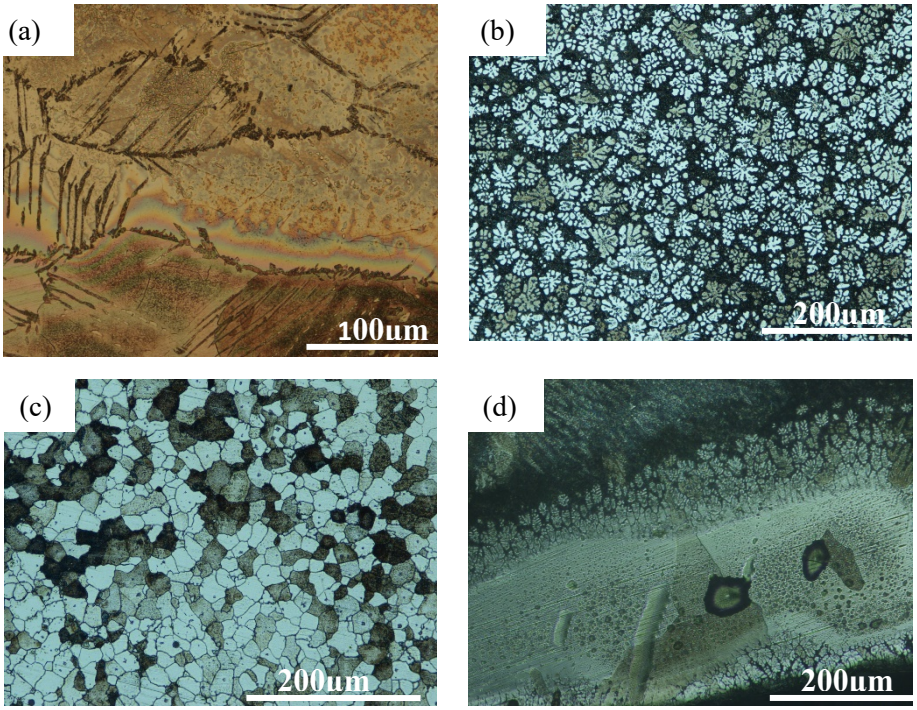

Figure 6. Microstructure of welds processed with different concentrations of mixture of aluminium + titanium powders at an energy input of 452J/mm: (a) CW, (b) 0.26 mg/mm², (c) 0.40 mg/mm² and (d) 0.55 mg/mm²

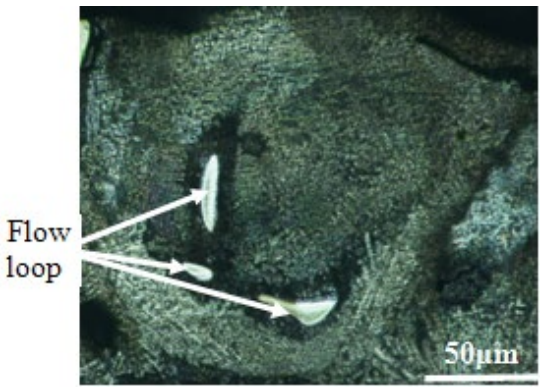

Figure 7. Microstructure of melt pool showing the flow loop

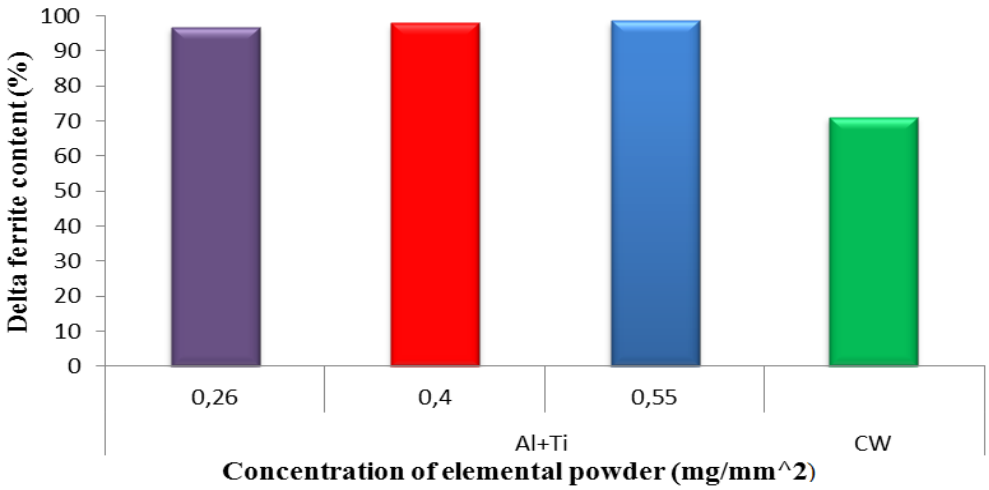

Figure 8. Delta ferrite content in melt pool treated with powder mixture

3.4 Grain Size of Powder Mixture Treated Welds

The grain size of the welds under different concentrations of powder mixture measured using quantitative microscopy based on Abrams Three Circle procedure with IMT image analysis software is shown in Figure 9. The figure shows that the grain size in the powder mixture treated welds is less than 10 µm whereas in the conventional welds, the grain size is between 33-40µm. At the energy input of 336J/mm, the grain size is not influenced by the change in the concentration of the powder mixture. However, at an energy input beyond 336 J/mm, the grain size increases with increase in the concentration of powder mixture. While this is intriguing, it may be that the thicker layer of the powder mixture at higher concentration require greater amount of energy input to achieve complete melting of the powders in order to provide sufficient sites for heterogeneous nucleation. The refinement in grain size accomplished in powder mixture treated weld relative to the conventional weld is about 73 percent.

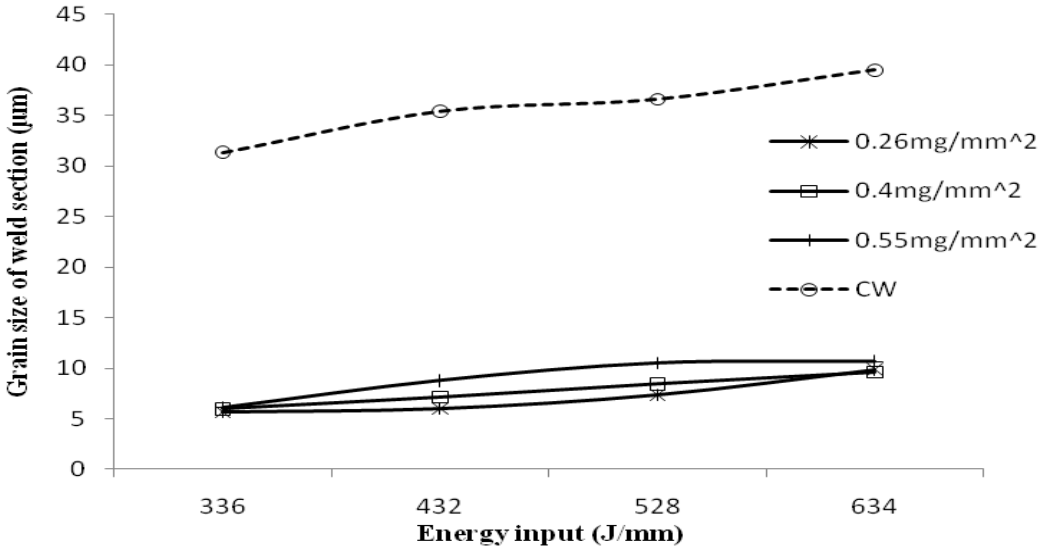

Figure 9. Combined effects of powder mixture and energy inputs on weld grain size

3.5 Mechanical Analysis

3.5.1 Microhardness

The hardness distribution across the resolidified melt pool measured at 1mm and 0.25mm intervals in both the transverse and thickness directions is shown in Figure 10. The hardness distribution in the traverse direction (Figure 10a) shows that the profile is higher than that of the conventional weld. The hardness in the weld is influenced by the concentration of the powder mixture. For 0.26 mg/mm^2 powder mixture, the maximum hardness was about 530 HV, and this increased to 600 HV when the concentration was increased to 0.40 mg/mm^2. However, the maximum hardness in the weld decreased to about 550 HV at 0.55 mg/mm^2 concentration of powder mixture. At this concentration of powder mixture, there was incomplete melting of the preplaced powder resulting in lower hardness. The hardness profile exhibited clear delineation between the weld regions and the base metal. The hardness distribution in the thickness direction shown in Figure 10b shows the profile increasing from the top surface through the thickness direction to the bottom surface with the conventional weld exhibiting the least value. The hardness value at the top surface varies for the different concentrations of the mixture of aluminum and titanium. The value is about 530HV for 0.26 mg/mm^2, 500HV for 0.40 mg/mm^2, and 550HV for 0.55mg/mm^2 of powder mixture, respectively. However, at the

bottom surface the hardness value converged to a constant value of about 600Hv relative to about 200 HV in conventional welds.

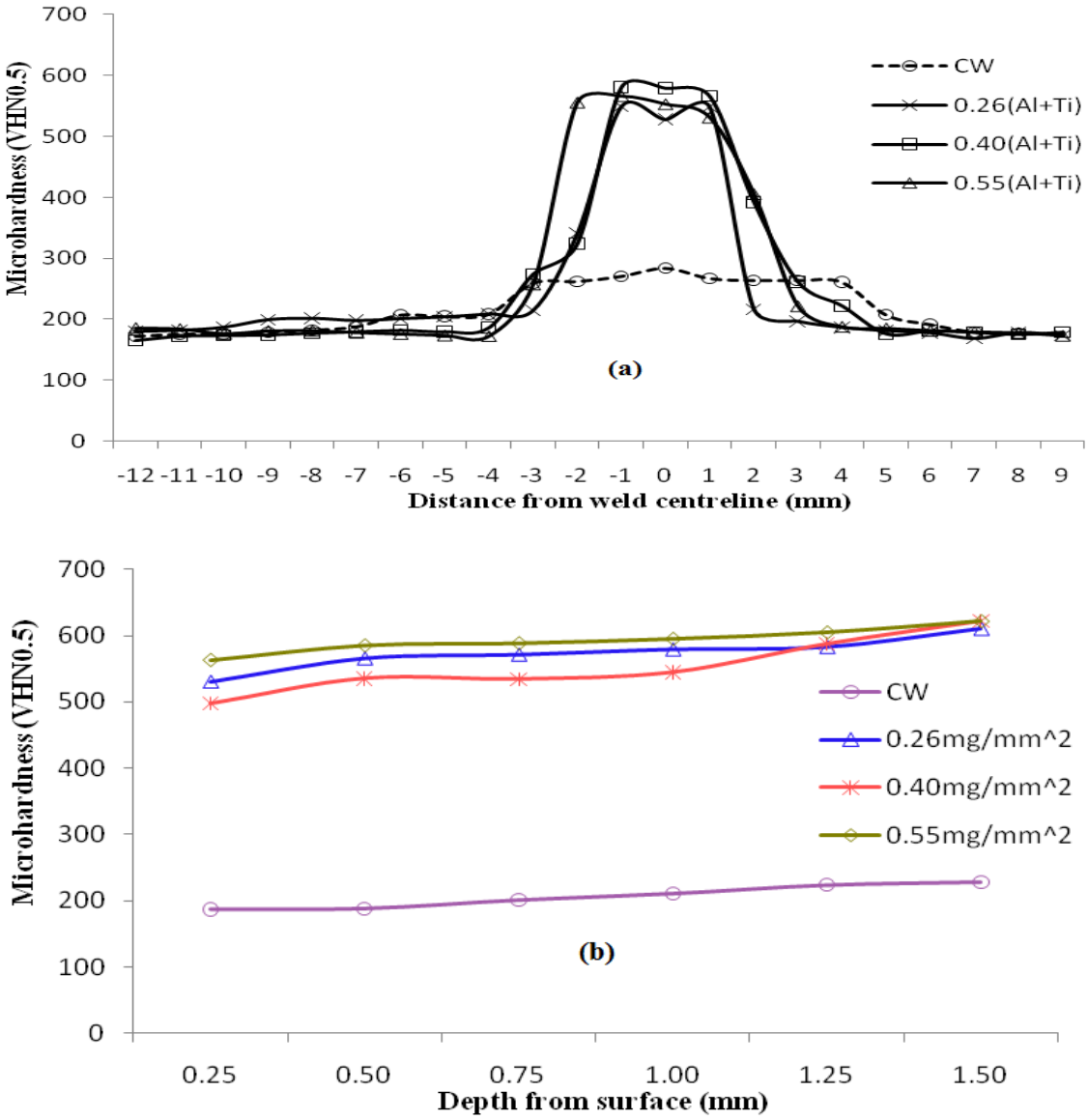

Figure 10. Hardness distribution in welds treated with Al and Ti powder mixture in relation to conventional welds: (a) Traverse hardness distribution and (b) hardness distribution in the thickness direction

3.5.2 Analysis of Tensile Strength of Powder Mixture Treated Welds

Figure 11 shows the tensile strenth curve for welds treated with different concentration of mixture of aluminum and titanium powders. The figure indicates that the strength values in the powder mixture treated weld is influenced by both concentration and energy input. For powder mixture concentration greater than 0.26 mg/mm^2, the conventional weld has a higher tensile strength across all energy inputs than the powder treated welds. However, the 0.26 mg/mm^2 powder mixture treated welds showed a higher tensile strength distribution within the energy input range 432-528 J/mm. But, beyond this range, the conventional weld exhibited higher tensile strength. A maximum strength of about 370 MPa was achieved in those welds treated

with 0.26 mg/mm^2 powder mixrure. The weld produced with an energy input of 336 J/mm exhibited the least tensile strength for all concentrations of powder mixture whilst that produced using an energy input of 528 J/mm gave the highest tensile strength across all concentrations of metal mixture powder. The relatively low value of tensile strength in the welds produced with 336 J/mm may be due to insuffient energy input to achieve the complete melting of the preplaced powder and homogenization of the melt pool. On the other hand, relatively high energy input represented by 634 J/mm leads to disolution of the grain pining precipitates resulting in grain growth in the welds. This ultimately results in reduction in the tensile strength of the welds.

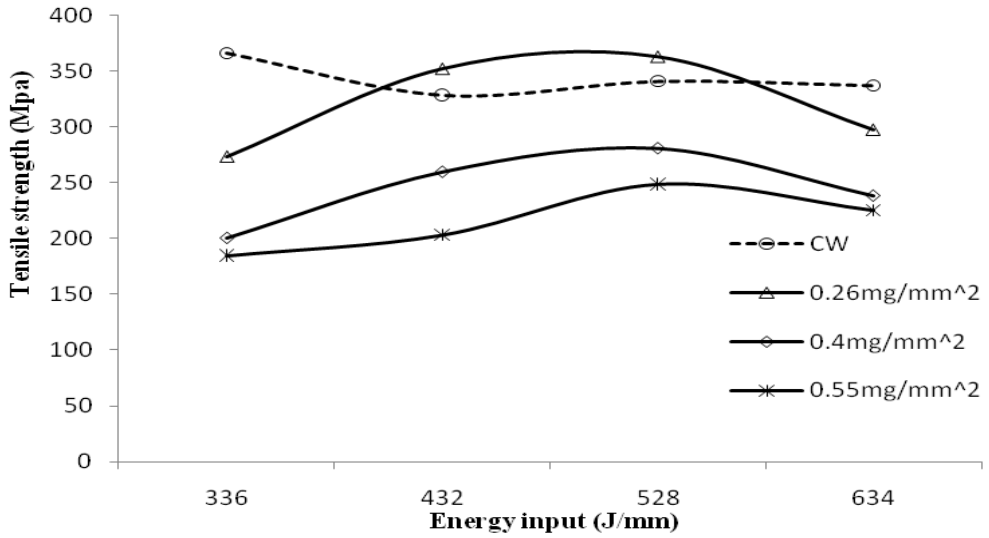

Figure 11. Combined effects of energy input and powder concentration on tensile strength of welds treated with mixture of aluminum and titanium powder

3.5.3 Influence of Grain Refinement on Weld Ductility

The effect of mixture of aluminum and titanium on the ductility of welds produced at different energy inputs is shown in Figure 12. It revealed that the welds treated with 0.55 mg/mm^2 powder mixture exhibited lower ductility curve across all energy inputs relative to the conventional weld. However, at 0.26 and 0.40mg/mm^2 of powder mixture, the ductility is energy input dependent. At an energy input lower than 432 J/mm, the ductility was higher than that in conventional weld whilst at an energy input greater than this, the ductility in the powder mixtrure treated welds was lower than in the conventional weld. The relative ductility shown in Figure 13 shows that powder mixture treated welds exhbits better ductility relative to the conventional welds. This is about 5 percent higher than that of the coventional weld but it is about 40 percent of the base metal. This concept for weld relative ductility for the evaluation of grain refinment strategies is well discussed in Amuda et al. (2018).

It appears that the grain morphology is not the only phenomenon controlling mechanical properties of ferritic stainless steel welds. Such other phenomena as the distribution of delta ferrite might equally be quite critical. Lippold and Kotecki (2005) had earlier reported that metallurgical features such as the presence of precipitate or delta ferrite might equally be significant on the after-weld properties of weld. In the present work, it appears that rather than

grain refinement, the mechanical properties of the powder mixture treated welds are influenced by the distribution of delta ferrite in the weld.

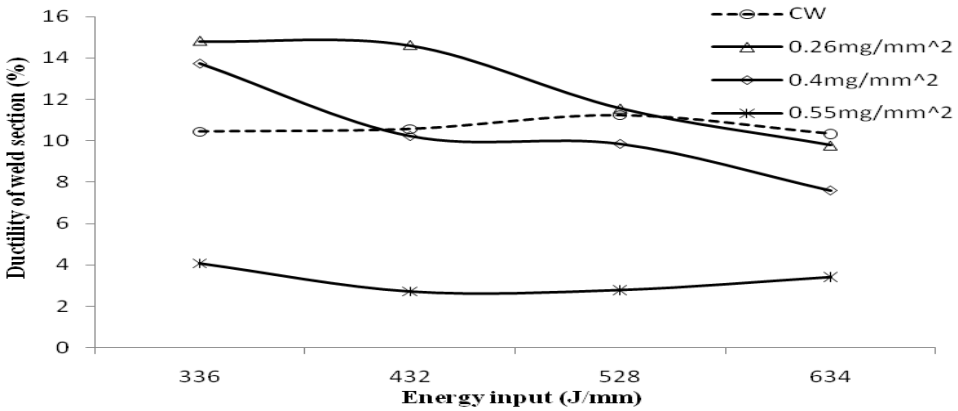

Figure 12. Ductility of powder mixture treated welds at different energy input

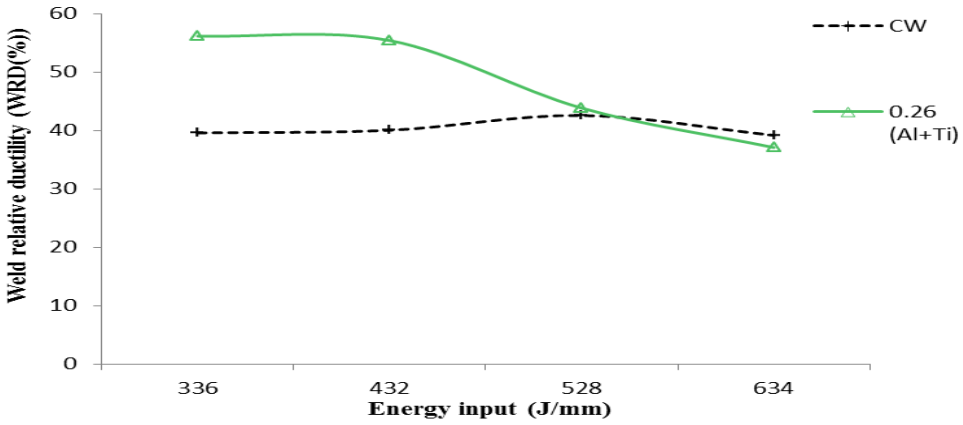

Figure 13. Weld relative ductility in powder mixture treated welds

3.5.4 Fractography of the Welds

The fractographs of powder mixture treated welds in relation to the conventional welds shown in Figure 14 indicate that whilst the fracture mode in conventional welds is quasi cleavage elongated in the director of fracture that in powder mixture treated welds exhibit mixed modes consisting of fibrous facets. The facets are essentially quasi equiaxed unlike the elongated columnar facet in the conventional welds.

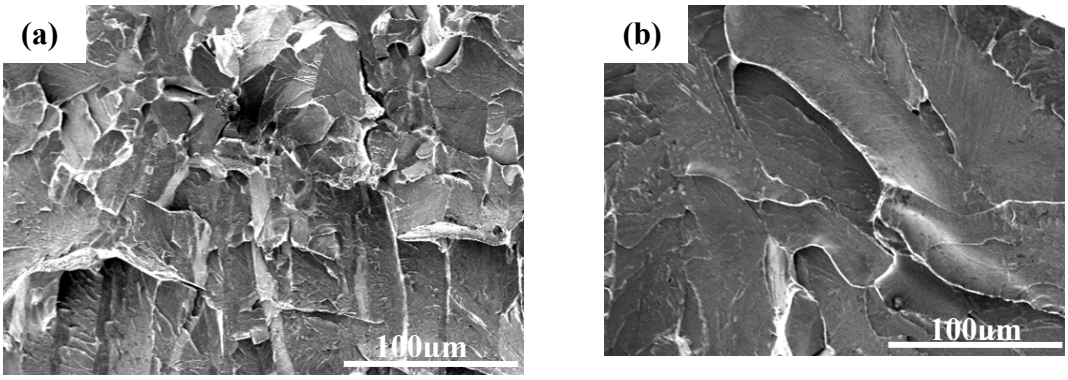

Figure 14. Tensile fractographs in powder mixture treated welds in relation to conventional weld: (a) powder mixture treated weld and (b) conventional weld

4.0 CONCLUSIONS

The microstructural evolution in medium chromium FSS welds treated with aluminum and titanium powder mixture has been characterized in relation to the mechanical properties of the weld. The study revealed that introduction of the powder mixture constricts the heat affected zone. The microstructure evolution in the powder treated welds transited from columnar elongated structure to refined equiaxed structure. Incorporation of powder mixture into the melt pool of the material increased the distribution of delta ferrite in the weld microstructure which may likely cause embrittlement in the weld. The constriction in bead size relative to the convention weld was about 43%. The degree of refinement in grain structure of the powder mixture treated welds was about 73%. The tensile and ductility of the powder mixture treated welds were 82 and 40 percent of the base metal, respectively. The ductility in the powder mixture treated weld is about 5 percent higher than that of the conventional weld at some concentrations of powder mixture. A major finding from the investigation was that introduction of the powder mixture produce defect free welds.

ACKNOWLEDGEMENT

This work was supported by the Research Management Office, International Islamic University Malaysia and represents the concluding part of a research on grain refinement in medium chromium FSS weld.

REFERENCES

Amuda, M. O. H. (2011). Microstructural features and properties of TIG melted AISI 430 ferritic stainless steel welds. Doctoral Thesis, International Islamic University Malaysia, Kuala Lumpur, Malaysia.

Amuda, M. O. H. and Mridha, S. (2010). Grain refinement in ferritic stainless steel welds: The journey so far. *Advanced Materials Research*, 83-86: 1165-1172.

Amuda, M.O.H., Akinlabi, E. T. and Mridha, S. (2017). Influences of energy input and metal powder addition on carbide precipitation in AISI 430 ferritic stainless steel welds. *Materials Today Proceedings*, 4**(2)**: 234-243.

Amuda, M.O.H., Akinlabi, E.T. and Mridha, S. (2016). Ferritic stainless steels: Metallurgy, Application and Weldability. In: Reference Module in Materials Science and Materials Engineering. Elsevier: New York, USA.

Amuda, M.O.H., Lawal, F.T., Onitiri, M.A., Akinlabi, E.T. and Mridha, S. (2018). Microstructure and Mechanical Properties of Metal Powder Treated AISI-430 FSS Welds. *International Journal of Manufacturing, Materials, and Mechanical Engineering (IJMMME)*, *8***(4)**: 63-83.

Anbazhagan, V. and Nagalakshmi, R. (2002). Metallurgical studies in ferritic stainless steel. *Welding Research Institute Journal*, 23(3):25–37.

Baldev, R., Kamachi Mudali, U., Vijayalakshmi, M., Mathew, M.D., Bhaduri, A.K., Chellapandi, P., Venugopal, S., Sundar, C.S., Rao, B.P.C. and Venkatraman, B. (2013). Development of Stainless Steels in Nuclear Industry: With Emphasis on Sodium Cooled Fast Spectrum Reactors History, Technology and Foresight. *Advanced Materials Research,* 794: 3-25.

Büyükyıldız, M., Kurudirek, M., Ekici, M., İçelli, O. and Karabul, Y. (2017). Determination of radiation shielding parameters of 304L stainless steel specimens from welding area for photons of various gamma ray sources. *Progress in Nuclear Energy*, 100: 245-254.

Cavazos, J.L. (2006). Characterization of precipitates formed in ferritic stainless steel stabilized with Zr and Ti additions. Material Characterization, 56: 96-101.

Cortie, M., Du Toit, M. (2016). Stainless steels, Ferritic. In: Reference Module in Materials Science and Materials Engineering. Elsevier: New York, USA.

Delgado, A.J., Ambriz, R.R., Cuenca-Alvarez, R., Alatorre, N. and López, F.F. (2016). Heat input effect on the microstructural transformation and mechanical properties in GTAW welds of a 409L ferritic stainless steel. *Revista de Metalurgia*, 52 **(2)**:68-77.

Jozwik, P. and Bojar, Z. (2007). Analysis of grain size effect on tensile properties of Ni3Al-based intermetallic strips. *Archives of Metallurgy and Materials*, 2**(2)**: 321-327.

Kamerud, K.L., Hobbie, K.A. and Anderson, K.A. (2013). Stainless steel leaches nickel and chromium into foods during cooking. *Journal of Agricultural and Food Chemistry*, *61***(39)**: 9495-9501.

Klas, W. (2012). Weldability of steel. In: Welding Process Handbook. Woodhead Publishing Series in Welding and Other Joining Technologies. 2nd edition. 191-206.

Kou, S. (2003). Welding metallurgy. 2nd edn. John-Wiley & Sons, New Jersey.

Lancaster, J. F. (1993). Metallurgy of welding, 5th edn. Chapman & Hall, London.

Lippold, J. C. and Kotecki, D. J. (2005). Welding metallurgy and weldability of stainless steel, New Jersey: Wiley-Interscience.

Lo, K.H., Shek, C.H. and Lai, J.K.L. (2009). Recent developments in stainless steels. *Materials Science and Engineering: R: Reports*, 65**(4-6)**: 39-104.

Morris Jr., J. W. (2001). The influence of grain size on the mechanical properties of steel. Retrieved on May 29, 2019. http://www.osti.gov/bridge/servlets/purl/861397-Tb7pb9/861397.pdf.

Mridha, S. and Baker, T.N. (1994). Crack-free hard surfaces produced by laser nitriding of commercial purity titanium. *Materials Science and Engineering A*, *188***(1-2)**: 229-239.

Mridha, S., Ong, H.S., Poh, L.S. and Cheang, P. (2001). Intermetallic coatings produced by TIG surface melting. *Journal of Materials Processing Technology*, *113***(1-3)**: 516-520.

Sarker, D. (2010). Hard coating layer formation on plain carbon steel surfaces by powder preplacement and TIG torch melting techniques, unpublished, Masters Thesis, International Islamic University Malaysia, Gombak, 2010.

Shahid, Z., Muhammad, A., Khattak, M., and Nasir, T. (2018). Effects of welding on the microstructural properties of AISI 430 ferritic stainless steel. *Journal of Advanced Research in Materials Science*, 44**(1)**: 25-32.

Villafuerte, J.C., Pardo, E. and Kerr, H.W. (1990). The effect of alloy composition and welding conditions on columnar-equiaxed transitions in ferritic stainless steel gas-tungsten arc welds. *Metallurgical Transactions A*, *21***(7)**: 2009 – 2019.